MicroRNA-214 protects the mouse heart from ischemic injury by controlling Ca^{2+} overload and cell death

Arin B. Aurora,[1] Ahmed I. Mahmoud,[2] Xiang Luo,[2] Brett A. Johnson,[1] Eva van Rooij,[3] Satoshi Matsuzaki,[4] Kenneth M. Humphries,[4] Joseph A. Hill,[2] Rhonda Bassel-Duby,[1] Hesham A. Sadek,[2] and Eric N. Olson[1]

[1]Department of Molecular Biology and [2]Department of Internal Medicine, The University of Texas Southwestern Medical Center, Dallas, Texas, USA. [3]miRagen Therapeutics, Boulder, Colorado, USA. [4]Free Radical Biology and Aging Program, Oklahoma Medical Research Foundation, Oklahoma City, Oklahoma, USA.

Early reperfusion of ischemic cardiac tissue remains the most effective intervention for improving clinical outcome following myocardial infarction. However, abnormal increases in intracellular Ca^{2+} during myocardial reperfusion can cause cardiomyocyte death and consequent loss of cardiac function, referred to as ischemia/reperfusion (IR) injury. Therapeutic modulation of Ca^{2+} handling provides some cardioprotection against the paradoxical effects of restoring blood flow to the heart, highlighting the significance of Ca^{2+} overload to IR injury. Cardiac IR is also accompanied by dynamic changes in the expression of microRNAs (miRNAs); for example, miR-214 is upregulated during ischemic injury and heart failure, but its potential role in these processes is unknown. Here, we show that genetic deletion of miR-214 in mice causes loss of cardiac contractility, increased apoptosis, and excessive fibrosis in response to IR injury. The cardioprotective roles of miR-214 during IR injury were attributed to repression of the mRNA encoding sodium/calcium exchanger 1 (Ncx1), a key regulator of Ca^{2+} influx; and to repression of several downstream effectors of Ca^{2+} signaling that mediate cell death. These findings reveal a pivotal role for miR-214 as a regulator of cardiomyocyte Ca^{2+} homeostasis and survival during cardiac injury.

Introduction

Cardiovascular disease affects more than 80 million people in the United States and is the leading cause of death in the developed world (1). Recent studies have revealed that microRNAs (miRNAs) play an indispensable role in various facets of cardiac function through their repression of target mRNAs (2). miRNAs exert their repressive functions by binding to sequences in the 3′-UTRs of target mRNAs that have complementarity to nucleotides 2–8 of the miRNA, known as the seed region. miRNAs mediate numerous cellular processes associated with cardiac remodeling and disease, including myocyte hypertrophy (3–9), fibrosis (10–13), angiogenesis (14–16), and apoptosis (17–21).

Cardiac ischemia, typically as a consequence of vessel occlusion, is often followed by a second set of stresses during restoration of blood flow to the tissue, known as ischemia/reperfusion (IR) injury, which can account for up to half of total infarct size (22). The factors contributing to IR injury are complex and include microvascular dysfunction, inflammation, release of oxygen radicals, disruption of Ca^{2+} homeostasis, and activation of mitochondrial apoptosis and necrosis. Cardiac failure results from the cardiomyocyte dropout brought about by these sequelae. Several miRNAs have been implicated in IR injury (19–21, 23–25), but there have been no genetic loss-of-function studies demonstrating the mechanism of action of individual miRNAs in this pathological process.

Ca^{2+} is central to cardiac contraction and to the signaling networks that regulate pathological cardiac growth and remodeling. Intracellular Ca^{2+} overload can occur in cardiomyocytes as a consequence of ischemic injury or other stresses, leading to contractile dysfunction and ultimately cell death (26, 27). Ca^{2+} handling is orchestrated by a set of proteins, including the L-type calcium channel sarco/endoplasmic reticulum Ca^{2+}-ATPase (SERCA2) pump, ryanodine receptor (RyR) channel, and sodium/calcium exchanger 1 (NCX1). Attenuation of Ca^{2+} overload with therapeutics targeting these proteins provides cardioprotection in some settings of IR (28–30), but clinical trials are limited by variables such as the effects of chronic inhibition of Ca^{2+} handling and timing of administration, and therefore future studies are needed to justify the usefulness of such treatments. The uncertainties surrounding these therapies highlight the importance of understanding the regulatory mechanisms that govern Ca^{2+} handling protein expression and function (31).

Ca^{2+} overload leads to cardiomyocyte death via signals transmitted through downstream effectors of Ca^{2+} handling (32). One intracellular sensor of Ca^{2+} ions, calmodulin, interacts through the calcium/calmodulin-dependent protein kinases (CaMKs) to regulate cardiomyocyte function and control cardiac hypertrophy and heart failure (32). Both apoptosis and necrosis can contribute to cardiomyocyte loss in response to Ca^{2+} overload by activating prodeath members of the Bcl2 family and opening the mitochondrial permeability transition (MPT) pore, respectively (26).

By analyzing conserved miRNAs that were upregulated in multiple disease models of hypertrophy and heart failure, we identified miRNA-214 (miR-214) as a sensitive marker of cardiac stress (5). Here we show that miR-214 plays a protective role against IR injury by attenuating Ca^{2+} overload–induced cardiomyocyte death through repression of NCX1 and downstream effectors of Ca^{2+} signaling and cell death. These findings provide new insights into the

Conflict of interest: Eric N. Olson and Eva van Rooij are cofounders of miRagen Therapeutics, a company focused on developing miRNA-based therapies for cardiovascular disease.

Citation for this article: *J Clin Invest.* 2012;122(4):1222–1232. doi:10.1172/JCI59327.

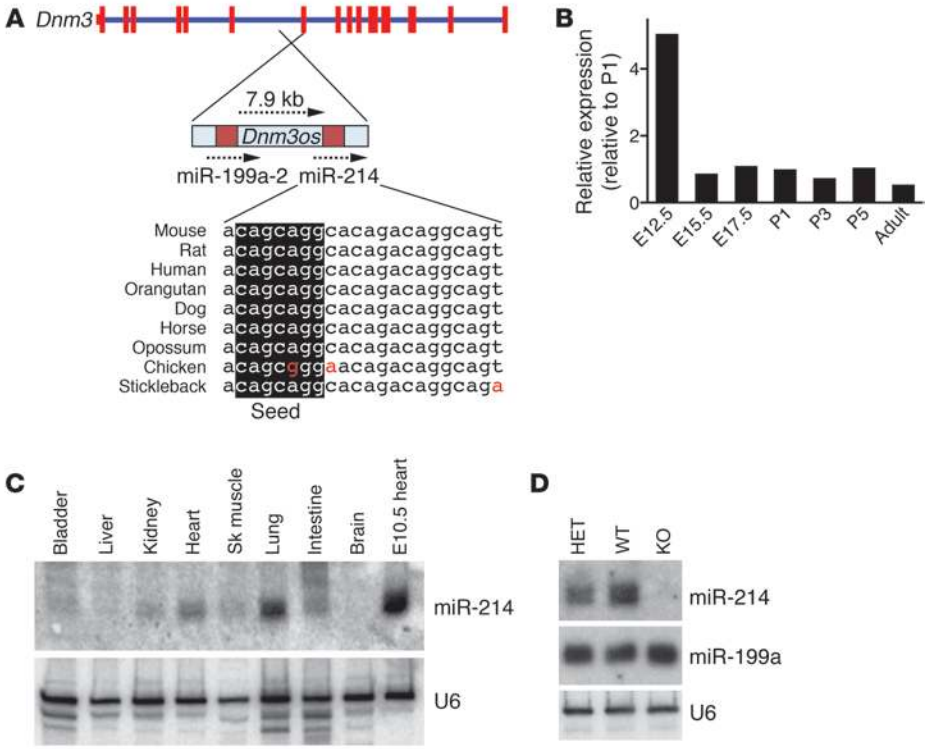

Figure 1
miR-214 genomic structure and genetic deletion. (**A**) Schematic representation of the mouse *miR-214* locus and its host gene, *Dnm3*. Boxes represent exons of the *Dnm3* gene. *miR-214* and *miR-199a-2* are clustered on the opposite strand within the non-coding RNA *Dnm3os*. Conservation of miR-214 is shown, and the seed region is highlighted. (**B**) miR-214 expression levels in the heart at various embryonic and postnatal stages according to miR-214–specific RT and qPCR. Data were normalized to RNU6B and expressed relative to levels at P1. (**C**) Northern blots show the relative expression level of miR-214 in WT adult mouse tissues. E10.5 heart RNA is included as a reference. U6 is a loading control. Blot is representative of 2 different sets of tissues analyzed. (**D**) Absence of miR-214 and preservation of miR-199a expression in KO hearts as shown by representative Northern blot from heart tissue of WT, heterozygous (HET), or miR-214 KO mice. U6 is a loading control. Sk, skeletal.

molecular basis of heart disease and point to miR-214 as a potential therapeutic target in this setting.

Results

miR-214 genomic structure and expression. miR-214 is highly conserved across vertebrates and is encoded within a larger non-coding RNA, Dnm3 opposite strand (*Dnm3os*). It is transcribed together with miR-199a-2 from the opposite strand of the *Dnm3* gene on mouse chromosome 1 (Figure 1A). miR-214 is upregulated in response to a variety of cardiac stresses, including pressure overload, myocardial infarction (MI), and overexpression of the calcium/calmodulin-sensitive phosphatase calcineurin (5, 12). Since many genes activated during cardiac stress are also expressed developmentally, we examined the temporal expression pattern of miR-214. Robust expression of miR-214 at early embryonic stages in the heart (Figure 1B) was downregulated by E15.5 and further decreased in adult mice. Expression could be detected in several adult tissues by Northern blot analysis (Figure 1C).

Targeted deletion of miR-214 in mice. To explore the functions of miR-214 in vivo, we used homologous recombination to generate a conditional targeted deletion of the gene in mice. Our targeting strategy introduced loxP sites flanking the genomic region encompassing the 106-bp pre-miR and a neomycin resistance cassette (Supplemental Figure 1A; supplemental material available online with this article; doi:10.1172/JCI59327DS1). Chimeric mice obtained from targeted ES cells transmitted the mutant allele through the germline, yielding mice heterozygous for *miR-214*$^{(neo)}$ (Supplemental Figure 1B). We bred these mice to CAG-Cre transgenic mice to remove the neomycin cassette and targeted region of the *miR-214* locus. Breeding of the offspring of these crosses generated homozygous *miR-214* KO mice, which were born at Mendelian ratios and were fertile (Supplemental Table 1). miR-214 KO mice displayed a minimal, but not statistically significant, reduction in body weight compared with WT littermates (Supplemental Figure 2A). Northern blot analysis confirmed the absence of miR-214 expression in the heart (Figure 1D), while the expression of miR-199a was preserved. Expression of miR-199a-2 in miR-214 KO mice was confirmed by quantitative real-time PCR (qPCR). Expression of the *Dnm3* host gene on the opposite strand was also maintained (Supplemental Figure 1C). RT-PCR spanning the entire *Dnm3os* transcript in WT and miR-214 KO mice verified that splicing of the long non-coding RNA was not disrupted (Supplemental Figure 1D).

miR-214 mutant mice have normal cardiac structure and function at baseline. Hearts of miR-214 KO mice at 8, 12, and 24 weeks appeared normal by gross examination and histological analysis (Figure 2A and data not shown). Heart weight/body weight and heart weight/tibia length ratios, cardiomyocyte size, and cardiac function were also indistinguishable between miR-214 KO and WT littermates at 8–12 weeks of age (Figure 2A, Figure 3C, and Supplemental Figure 2C). We examined expression of collagen and fetal cardiac genes as an indication of underlying defects in the hearts of adult miR-214 KO mice, but saw no significant differences from WT (Figure 2B). Sarcomere structure and mitochondrial structure and volume also appeared normal in the miR-214 KO hearts, as assessed by electron microscopy (Figure 2C and Supplemental Figure 2B). We performed similar analyses of hearts from 10- to 12-month-old miR-214 KO mice and WT littermates and saw no significant differences in heart/body weight ratios, fetal gene expression profiles, cardiac function, or cardiomyocyte size upon aging (Supplemental Figure 3, A–D).

While the above data did not show differences between WT and miR-214 KO mice, microarray analysis of hearts from miR-214 KO and WT littermates at 2 and 8 weeks of age revealed that several

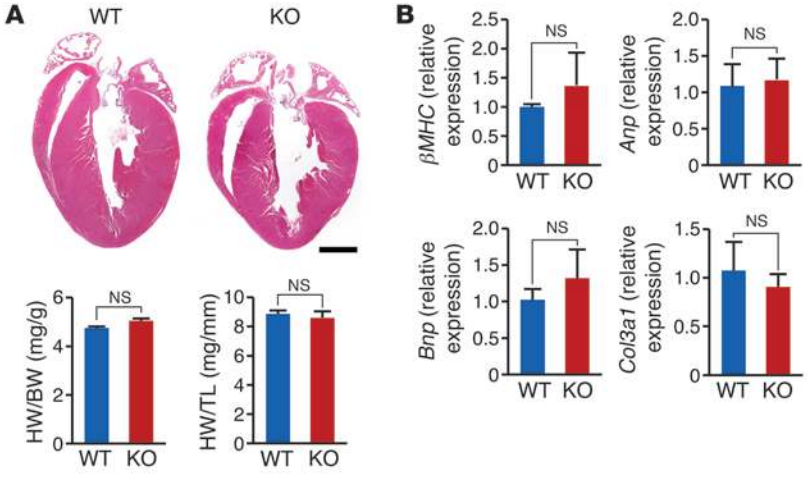

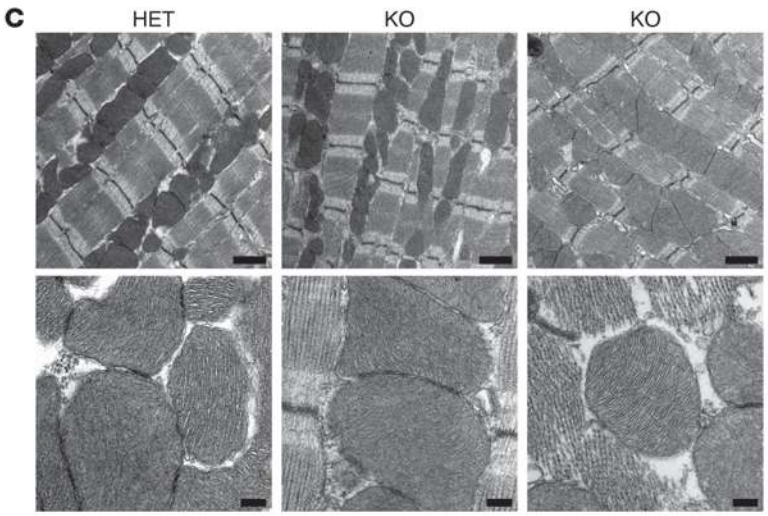

Figure 2
Normal cardiac structure and function in miR-214 KO mice at baseline. (**A**) Heart sections stained with H&E from WT and miR-214 KO mice at 8 weeks of age. Heart weight/body weight (HW/BW) and heart weight/tibia length (HW/TL) ratios shown are representative of adult mice at 3 different ages. Mean values ± SEM; $n = 3$. Scale bar: 2 mm. (**B**) qPCR expression analysis of cardiac stress response genes in miR-214 KO hearts relative to WT. $n = 3$ per group; data are representative of 2 separate experiments. Data are shown as fold induction of gene expression normalized to 18S and expressed as mean ± SEM. (**C**) Representative electron microscopy images from a miR-214 heterozygote and 2 miR-214 KO hearts at 8 weeks of age highlighting sarcomeric structure and mitochondria. Scale bars: 1 μm (top row) and 200 nm (bottom row).

metabolic and Ca^{2+}-handling genes were upregulated in miR-214–deficient hearts (Supplemental Table 2).

miR-214 protects mice against IR injury. The altered metabolic and Ca^{2+}-handling microarray profiles of miR-214 KO hearts led us to hypothesize that the mutant mice might respond differently to ischemic cardiac injury. Indeed, permanent ligation of the left anterior descending coronary artery (LAD) in mice, which induces MI, resulted in a significant increase in mortality in miR-214 KO mice compared with WT controls (Figure 3A). Transient ligation of the LAD in mice causes cardiomyocyte loss and impaired cardiac function that mimics the pathology seen in IR injury in human hearts. By Northern blot analysis, we observed upregulation of miR-214 in the hearts of WT mice subjected to 45 minutes of ischemia and 1 or 7 days of reperfusion (Figure 3B). We tested the response of miR-214 KO mice to the same IR procedure. Indeed, miR-214 KO mice displayed severely impaired cardiac function 7 days after reperfusion, as measured by transmural echocardiography, while WT controls showed a minimal functional deficit (Figure 3C).

The extent of myocyte loss, fibrosis, and impairment of cardiac performance varies depending on the length of the ischemic period during IR. We found that 45 minutes of ischemia in WT mice resulted in transient myocyte apoptosis, detectable by TUNEL staining 24 hours later, but not at day 7 following IR. In contrast, miR-214 KO hearts had higher numbers of TUNEL-positive cells after both 24 hours and 7 days of reperfusion (Figure 3D). We used desmin staining to visualize TUNEL-positive cardiomyocytes (Figure 3D). Apoptotic myocytes disassemble their sarcomeres and downregulate contractile proteins; therefore, desmin staining in most of the TUNEL-positive areas was relatively dim.

To further assess the response of miR-214 KO mice to IR, we examined cardiomyocyte size and fibrosis. Wheat germ agglutinin staining of heart sections after 7 days of reperfusion showed a slight increase in cardiomyocyte size in miR-214 KO mice compared with WT controls (Supplemental Figure 4A). Masson's trichrome staining of hearts at day 7 of reperfusion revealed small areas of fibrosis in WT hearts, while miR-214 KO hearts contained larger fibrotic regions (Figure 3E). These findings suggest that increased and sustained apoptosis in miR-214 KO mice after IR triggers extensive fibrosis and impaired cardiac function.

IR injury initiates a complex cycle of hypoxia and cell death that is perpetuated by inflammation, production of oxygen radicals, Ca^{2+} overload, and activation of mitochondrial apoptosis (22). Histological examination of miR-214 KO and WT hearts after 24 hours of reperfusion revealed no differences in the numbers of infiltrating leukocytes (Supplemental Figure 4B). At baseline, mitochondrial morphology and number also appeared unchanged in the KO mice (Figure 2C). Enzymatic assays for electron transport chain activity and superoxide production showed no differences between WT and miR-214 KO mitochondria at baseline or at multiple time points after reperfusion (Supplemental Figure 5, A–D). We therefore investigated the possibility that Ca^{2+} homeostasis was regulated by miR-214.

Regulation of NCX1 by miR-214. While Ca^{2+} is a central mediator of excitation-contraction coupling of cardiomyocytes, ischemic injury causes intracellular Ca^{2+} overload, leading to contractile dysfunction and ultimately cell death (26, 27). To identify candidate miR-214 targets involved in Ca^{2+} regulation, we used the prediction algorithm TargetScan (http://www.targetscan.org/). One of the top predicted targets of miR-214 was the sodium/calcium exchanger *Slc8a1* (i.e., *Ncx1*) mRNA. Under normal conditions,

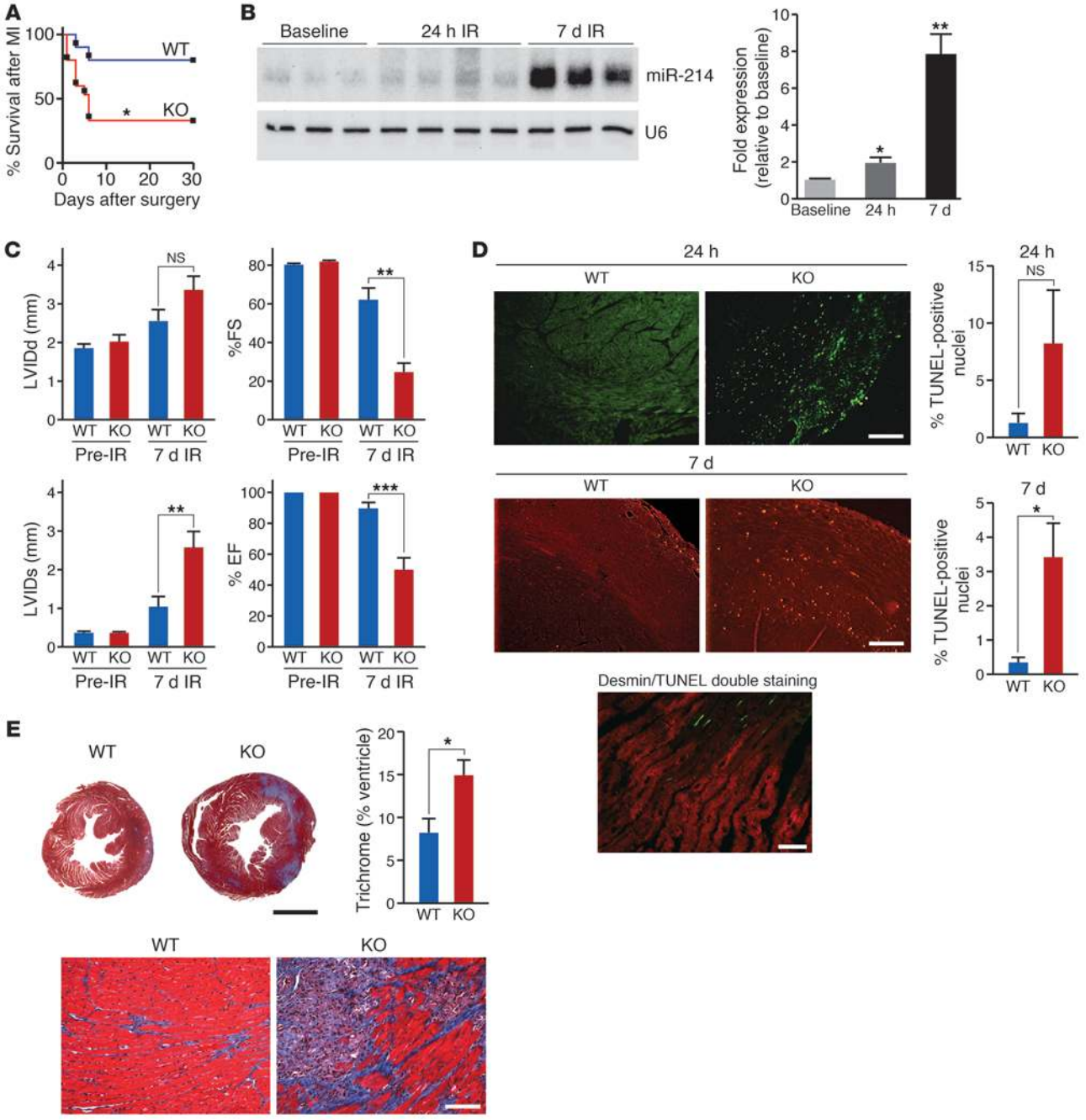

Figure 3

miR-214 protects the heart against MI and IR. (**A**) Survival curve following MI (permanent LAD ligation) in miR-214 KO mice or WT littermates. n = 13–15, data represent mice from 3 different experiments. *P < 0.05. (**B**) Northern blotting and quantification of miR-214 expression in WT hearts at baseline and following IR. miR-214 levels were normalized to U6 loading control and expressed relative to baseline. *P = 0.04, **P < 0.01. (**C**) Cardiac function in WT and miR-214 KO mice before and after IR (7 days reperfusion). Quantification of left ventricular internal diameter in systole or diastole (LVIDs or LVIDd), fractional shortening (FS) and ejection fraction (EF), is shown. n = 6; data represent mean ± SEM of 3 independent experiments. **P < 0.01, ***P < 0.001. (**D**) TUNEL staining in heart sections following IR. Representative images at 24 hours and 7 days of reperfusion are shown. Scale bar: 200 μm. The percentage of TUNEL-positive nuclei was calculated. For each mouse, sections at 3 different levels (6–8 fields per section) were counted. Bottom: Simultaneous TUNEL (green) and desmin staining (red) from miR-214 KO heart sections following IR. Scale bar: 40 μm. (**E**) Masson's trichrome staining on transverse heart sections after 7 days of reperfusion. Representative images shown at two different magnifications. Scale bars: 2 mm (top), 100 μM (bottom). The area of blue staining was quantified (3 section levels per heart) and expressed as a percentage of total area. For **D** and **E**, mean ± SEM; n = 3; *P < 0.05.

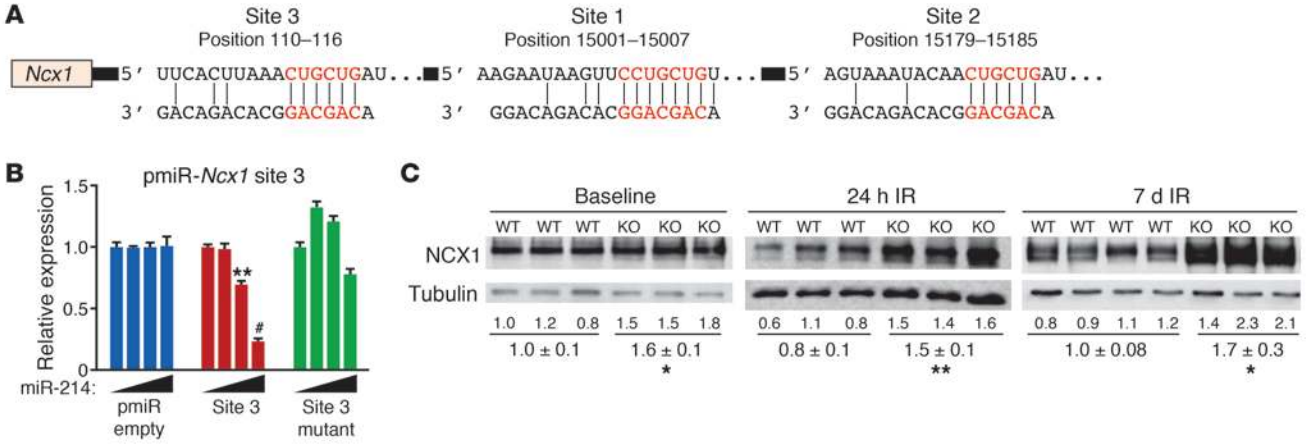

Figure 4

miR-214 regulates NCX1. (**A**) Predicted miR-214 binding sites in the 3′-UTR of *Ncx1* mRNA. *Ncx1* contains 3 conserved sites. Site position relative to beginning of the 3′-UTR is indicated above. Seed and target sequences are highlighted in red, and base pairing between miR-214 and target site marked by vertical lines. (**B**) Ability of miR-214 to directly repress activity of the luciferase reporter construct that contains the portion of the *Ncx1* 3′-UTR that includes site 3 (pmiR-*Ncx1* site 3). WT and mutant *Ncx1* 3′-UTR sequences were tested. Black triangles indicate increasing amounts of transfected miR-214 expression plasmid (0, 50, 100, and 200 ng). Luciferase activity was normalized to β-galactosidase activity and compared with empty vector measurements (pmiR empty). Luciferase assays were performed in triplicate and are representative of 2–3 independent experiments. Data are mean ± SEM. $^{**}P < 0.01$, $^{\#}P < 0.001$. (**C**) NCX1 protein levels measured by immunoblotting in whole heart lysates from miR-214 KO mice compared with WT at baseline and after IR (24 hours and 7 days). Quantification was normalized to tubulin as a loading control and then compared with WT. Data are representative of 2 independent experiments. Mean ± SEM; $n = 3$. $^{*}P < 0.04$, $^{**}P < 0.01$.

NCX1 is the primary pump by which Ca^{2+} is extruded from cardiomyocytes during relaxation; but during stress, the exchanger contributes to Ca^{2+} overload by operating in reverse mode, resulting in an increased concentration of intracellular Ca^{2+} (33).

The 3′-UTR of *Ncx1* mRNA is greater than 15 kb in length and contains 3 conserved miR-214 binding sites (sites 1–3) (Figure 4A). To test whether miR-214 could repress these predicted sequences, we co-transfected cells with constitutively active luciferase reporter constructs containing regions of the *Ncx1* 3′-UTR and miR-214 expression plasmid. Since site 3 is almost 15 kb away from sites 1 and 2 in the 3′-UTR of the *Ncx1* mRNA, we made two different pmiR reporter constructs: construct 1 contained sites 1 and 2, and construct 2 contained site 3. We observed dose-dependent repression of luciferase activity by miR-214 for the *Ncx1*-UTR reporter containing site 3, and repression was abolished by mutagenesis of the seed-binding region (Figure 4B). miR-214 also repressed activity of the reporter containing sites 1 and 2 but was not affected by mutation of either or both sites (Supplemental Figure 6A). However, this construct contained several non-conserved sequences that have 6-nucleotide complementarity to the miR-214 seed and therefore likely act as additional sites for repression.

At baseline, we observed a significant increase in NCX1 protein expression in miR-214 KO hearts (Figure 4C). NCX1 protein levels in miR-214 KO hearts were also greater than in WT littermates at 24 hours and 7 days of reperfusion (Figure 4C), suggesting that NCX1 is a direct target of miR-214 repression. To assess absolute changes in NCX1 levels after IR, we performed a side-by-side analysis of littermate samples from miR-214 KO and WT mice at baseline and at 24 hours and 7 days after IR (Supplemental Figure 6, B–D). In WT mice, NCX1 levels rose slightly at 24 hours after IR and then significantly dropped by 7 days to levels below baseline. In contrast, in miR-214 KO hearts, NCX1 levels (which were increased at baseline compared with WT) significantly increased at 24 hours after IR and did not significantly drop at day 7 (Supplemental Figure 6D). Together, these findings suggest that in the absence of miR-214, uncontrolled increases in NCX1 lead to greater myocyte apoptosis and injury during IR.

miR-214 regulation of Ca^{2+} signaling and cell death. Many miRNAs mediate stress responses by fine-tuning multiple target mRNAs that function in the same or parallel pathways within a cell. Therefore, we assessed other potential miR-214 targets that might contribute to cardiomyocyte death following IR by sensing Ca^{2+} overload or mediating apoptosis. Three additional miR-214 target candidates were identified. *Bcl2l11* (BCL2-like 11 or *Bim*) is a proapoptotic Bcl2 family member predicted to have four miR-214 binding sites: one highly conserved (site 4), one conserved through primates (site 3), and two non-conserved sites (sites 1 and 2) (Figure 5A). The mRNA encoding CaMKIIδ, which can drive cardiac hypertrophy (34) and has been implicated in apoptosis and IR injury (35, 36), contains one highly conserved predicted miR-214 site (Figure 5A). The mRNA encoded by *Ppif* (the gene encoding cyclophilin D) contains one predicted miR-214 site (Figure 5A). Cyclophilin D (CypD) is a major regulator of the MPT pore required for mediating Ca^{2+}- and oxidative damage–induced cell death independent of the Bcl2 family pathway (37–40).

To test whether miR-214 could repress protein expression through these predicted binding sites, we co-transfected cells with constitutively active luciferase reporter constructs containing the 3′-UTR sequences for *Ppif*, *Bim*, or *CamkIId* and miR-214 expression plasmid. miR-214 significantly repressed the activity of the *CamkIId* and *Ppif* 3′-UTRs (Figure 5D), though we did not observe repression of luciferase activity with the *Bim* 3′-UTR construct in this assay (data not shown). Baseline protein levels of CypD, BIM, and CaMKIIδ were significantly elevated in miR-214 KO compared with WT hearts (Figure 5B). Following IR, we detected increased levels of BIM and CaMKIIδ in the miR-214 KO samples compared with controls

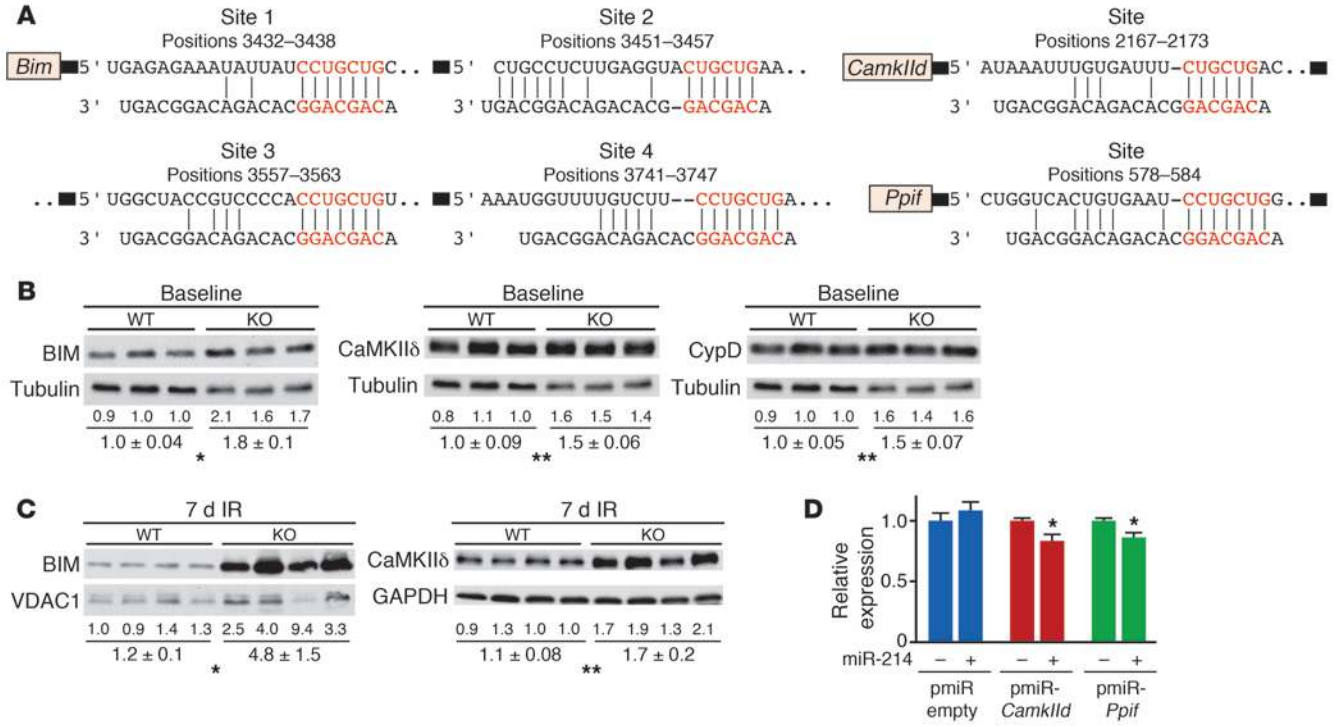

Figure 5

miR-214 regulation of Ca^{2+} signaling and cell death genes. (**A**) Predicted miR-214 binding sites in the 3′-UTR of *Bim*, *CamkIId*, and *Ppif* mRNA. *Bim* contains 4 predicted sites, while *CamkIId* and *Ppif* each contain one. Site position relative to beginning of the 3′-UTR is indicated above each panel. Seed and target sequences are highlighted in red and base pairing between miR-214 and target site marked by vertical lines. (**B** and **C**) Target protein levels measured by immunoblotting in whole heart lysates from miR-214 KO mice compared with control at baseline (**B**) and after IR (7 days) (**C**). Quantification is normalized to indicated loading control and then compared with WT. Data are representative of 2 independent experiments. Mean ± SEM; $n = 3$. $^*P < 0.05$, $^{**}P < 0.01$. (**D**) Ability of miR-214 to directly repress the activity of luciferase reporter constructs that contain the 3′-UTR for *CamkIId* and *Ppif* as indicated. Transfection with or without miR-214 expression plasmid is indicated. Luciferase activity was normalized to β-galactosidase activity and compared with empty vector measurements. Luciferase assays were performed in triplicate and are representative of 2–3 independent experiments. Data are mean ± SEM. $^*P < 0.05$.

(Figure 5C), but no changes at this time point for CypD (data not shown). Together, the data suggest that miR-214 may further protect the heart against IR injury by directly attenuating target genes that transmit Ca^{2+} overload signals and mediate cell death.

Aberrant Ca^{2+} handling in miR-214–deficient cardiomyocytes. The enhanced expression of NCX1 suggested that miR-214 maintains Ca^{2+} homeostasis in cardiomyocytes under conditions of stress. To further explore the influence of miR-214 on Ca^{2+} regulation, we isolated cardiomyocytes from adult miR-214 KO mice or WT controls and examined their Ca^{2+} handling activity at the single-cell level using Fura-2. At physiological extracellular Ca^{2+} concentrations (1.8 mM), a condition wherein NCX1 operates in Ca^{2+} efflux mode, the miR-214 KO cells had lower levels of intracellular Ca^{2+} transients compared with controls (Figure 6, A and B). We pulsed cardiomyocytes with 5 mM extracellular Ca^{2+} to reflect the environment in the heart during IR injury. In the presence of high extracellular Ca^{2+}, a condition wherein NCX1 operates in reverse mode, intracellular Ca^{2+} transients were increased in the miR-214 KO cells (Figure 6, A and B). Under both conditions, decay rates were similar between KO and WT cardiomyocytes. These findings suggest that cardiomyocytes deficient for miR-214 are sensitized to Ca^{2+} overload following IR injury as a consequence of elevated reverse mode NCX1.

miR-214–depleted cardiomyocytes are sensitized to IR-induced cell death. The Ca^{2+} abnormalities that occur during IR are complex and can include intracellular release from mitochondria. To further recapitulate these effects, we used an in vitro model of IR to confirm that miR-214 protects cardiomyocytes from Ca^{2+} overload and subsequent cell death by directly regulating NCX1 and other targets. First, isolated neonatal rat cardiomyocytes in culture were transfected with 15-nucleotide locked nucleic acid (LNA)–modified antimiRNAs against miR-214 (antimiR-214) or a 15-mer oligonucleotide control (against a *Caenorhabditis elegans* miRNA) (100 nM). Real-time PCR showed efficient knockdown of miR-214 expression in the antimiR-214 group compared with the 15-mer control at 72 hours after transfection (Figure 7A). We used two different models of in vitro IR to test the effects of miR-214 knockdown on IR-mediated apoptosis in cardiomyocytes by TUNEL staining: 2 hours of ischemia (5% CO_2, 1% O_2) followed by 24 hours of reperfusion (mild IR) and 1 hour of anoxia (5% CO_2, 0% O_2) followed by 4 hours of reperfusion (severe IR). Both IR conditions increased the percentage of TUNEL-positive cells among control transfected cardiomyocytes, while antimiR-214 treatment further increased apoptosis relative to control anti-miRNA (Figure 7, B and C). Knockdown of miR-214 expression also resulted in significant increases in *Ncx1*, *Bim*, *Ppif*, and *CamkIId* mRNAs, measured by qPCR (Figure 7D),

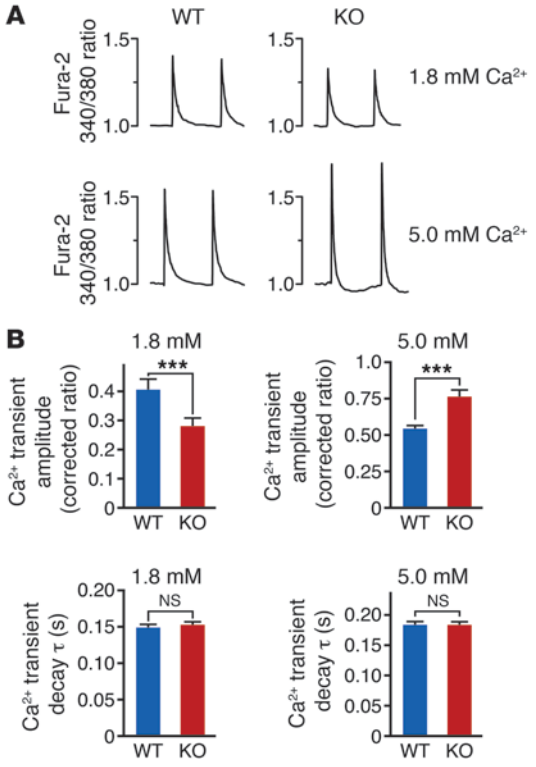

Figure 6
miR-214 is required to maintain efficient Ca^{2+} handling. (**A**) Representative Ca^{2+} traces obtained from isolated WT or miR-214 KO cardiomyocytes. Myocytes were imaged in the presence of 1.8 mM or 5.0 mM extracellular Ca^{2+}. n = 15–20 cells, with 3–5 animals per group for all experiments. (**B**) Quantitative analyses of intracellular Ca^{2+} levels shown as corrected average peak Ca^{2+} transients in WT and miR-214 KO cardiomyocytes in 1.8 mM or 5.0 mM extracellular Ca^{2+} (top). Ca^{2+} transient decay shown as τ (seconds) comparing WT and KO at 1.8 mM and 5.0 mM extracellular Ca^{2+} (bottom). All data are mean ± SEM; ***P < 0.0001.

supporting the in vivo evidence that they are direct miR-214 targets in cardiomyocytes. The target regulation we observed in vitro and subsequent sensitization to IR-induced apoptosis are supportive of both the in vivo IR phenotype and Ca^{2+} handling data showing enhanced reverse mode NCX1 activity in miR-214 KO cardiomyocytes subjected to high extracellular Ca^{2+}.

Discussion

The results of this study reveal miR-214 as a central, stress-responsive protector against excessive Ca^{2+} uptake and cardiomyocyte cell death both in vivo and in vitro. Mice deficient for miR-214 are sensitized to IR injury, evidenced by increased cardiac apoptosis and fibrosis and loss of pump function. miR-214 directly inhibits its *Ncx1* mRNA such that elevated NCX1 expression in miR-214 KO mice causes increased Ca^{2+} overload, consistent with reverse mode activity of the exchanger during IR. By inhibiting effectors of Ca^{2+} overload signaling pathways such as CaMKIIδ, CypD, and BIM, miR-214 can diminish the degree of cardiomyocyte death sustained during IR. Cardiomyocytes lacking miR-214 have impaired Ca^{2+} handling and an increased sensitivity to IR-induced apoptosis. A model to account for the role of miR-214 in mediating Ca^{2+} handling and cell death during ischemic injury is shown in Figure 8.

miR-214 protects the heart against IR injury. At baseline, miR-214 KO mice appear histologically and functionally normal, consistent with an increasing number of reports that individual miRNAs can be deleted in mice with minimal consequences under normal conditions (41). While studies in vitro and in zebrafish suggest that miR-214 controls skeletal muscle development (42, 43), we observed no skeletal muscle abnormalities in miR-214 KO mice. Mice lacking *Dnm3os*, a large non-coding RNA (lncRNA) that contains miR-214, display severe skeletal defects and die within the first month of birth, though the functions of *Dnm3os* have not been reported (44). Any potential role of miR-214 in this phenotype is difficult to discern, since the *Dnm3os* deletion also eliminates much of the lncRNA including miR-199a.

In contrast, miR-214 KO mice show impaired cardiac function and susceptibility to death following MI and IR injury. Multiple initiators in IR injury including inflammation, oxygen radicals, and Ca^{2+} overload contribute to the loss of cardiomyocytes and the progression to heart failure (27). The cardioprotective effects of miR-214 correlate with the repression of NCX1, CaMKIIδ, CypD, and BIM. However, miR-214 may have additional targets that contribute to its function during cardiac stress.

Ca^{2+} homeostasis during cardiac stress: regulation by miR-214 and NCX1. In WT mice, we found that NCX1 expression increased at 24 hours of reperfusion and then declined below baseline levels by 7 days (Supplemental Figure 6, B–D). Elevated miR-214 expression (Figure 3B) presumably counteracts upregulation of NCX1 and continues to increase such that by 7 days of reperfusion, miR-214 downregulation of NCX1 is sufficient to reestablish Ca^{2+} homeostasis in cardiomyocytes. In miR-214 KO hearts, NCX1 expression was elevated at baseline, predisposing cardiomyocytes to Ca^{2+} overload. Furthermore, without upregulation of miR-214 following IR, NCX1 levels continued to increase unchecked (Supplemental Figure 6, B–D).

NCX1 counter-transports sodium and Ca^{2+} across the sarcolemmal membrane and, at baseline conditions in the heart, is one of the major pathways through which intracellular Ca^{2+} effluxes out of cardiomyocytes. However, it is well documented that during various forms of cardiac stress, including IR injury, the NCX1 transporter works in reverse mode to pump Ca^{2+} back into the cell. Furthermore, reverse mode NCX1 can induce Ca^{2+}-induced Ca^{2+} release from the SR, leading to additional Ca^{2+} overload, injury, and cardiac dysfunction (45, 46).

Consistent with our model, transgenic mice that overexpress NCX1 in the heart phenocopy the exacerbated response to IR observed with miR-214 KO mice, ultimately resulting in reduced cardiac function and survival (47–49). NCX1 upregulation has also been observed in cardiac hypertrophy (50–52) in which miR-214 is also upregulated. Together, these findings suggest that repression of reverse mode NCX1 by miR-214 following IR attenuates Ca^{2+} overload and apoptosis in the heart and that a similar mechanism may be critical in other settings of cardiac stress.

High extracellular Ca^{2+} levels in vitro mimic conditions of cardiac stress such as IR, where cardiomyocytes are exposed to significant increases in Ca^{2+} from surrounding tissue. Interestingly, induced overexpression of NCX1 in cardiomyocytes leads to similar or lower levels of intracellular Ca^{2+} transients in the presence of physiological extracellular Ca^{2+}, but higher transients in the presence of high extracellular Ca^{2+} (53). In miR-214 KO myocytes, we observed similar results, suggesting that the increased expres-

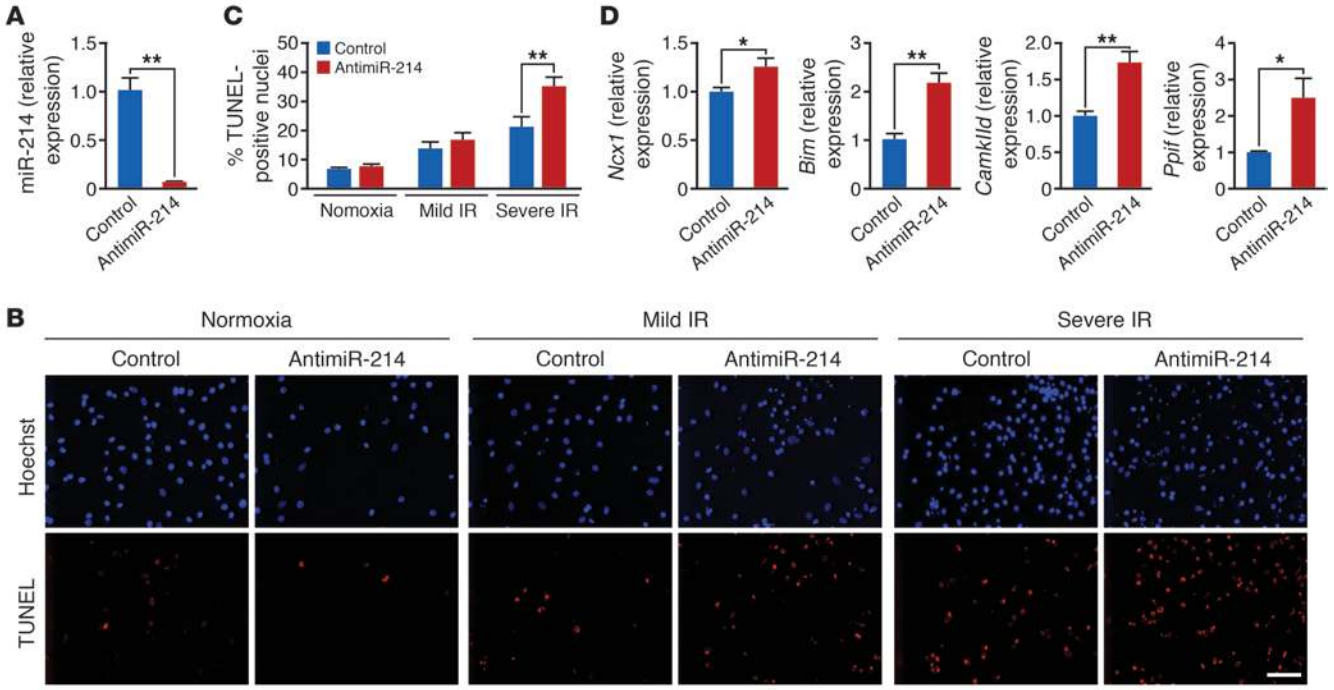

Figure 7

miR-214 protection of cardiomyocytes and regulation of target genes in vitro. (**A**) RNA isolated from neonatal rat cardiomyocytes transfected with antimiR-214 or 15-mer control (100 nM) was analyzed by miR-214–specific RT-PCR and qPCR to assess levels of miR-214 suppression. $^{**}P < 0.01$. (**B** and **C**) TUNEL staining of neonatal rat cardiomyocytes transfected with control or antimiR-214 and then subjected to in vitro simulation of IR. (**B**) Representative images of total nuclei (blue) and apoptotic nuclei (red) from normoxic and both IR conditions are shown for control and antimiR-214 transfected samples. Scale bar: 100 μm. (**C**) Quantification of percent TUNEL-positive nuclei. Samples were assayed in triplicate, and results are representative of 2–3 independent experiments. Data are mean ± SEM; $^{**}P < 0.01$. (**D**) Levels of miR-214 target mRNAs in cardiomyocytes transfected with antimiR-214 or control antimiR as indicated. Data were normalized to ribosomal 18S and expressed relative to control. Samples were run in triplicate, and results are representative of 2 independent experiments. All data are mean ± SEM; $^{*}P = 0.02$, $^{**}P < 0.01$.

sion of NCX1 in KO cells working in reverse mode contributes to Ca^{2+} overload. Since NCX1 can contribute to Ca^{2+} efflux during relaxation, one might expect to see an increased rate of transient decline with increased NCX1 expression. However, in our study and others, changes in NCX1 expression do not impact the rate of Ca^{2+} decline (refs. 53, 54, and Figure 6B). The variable effects on decline rate observed with NCX1 overexpression seem to depend on the species studied, differences in temperature, and the phase of the decline that was evaluated (55–57).

miR-214 regulation of Ca^{2+} signaling and cardiomyocyte death. Intracellular Ca^{2+} levels are modulated by the activity of numerous channels, pumps, and exchangers and then transduce signals to the cell through downstream effectors. Elevation in intracellular Ca^{2+} activates CaMKIIδ, the main isoform of CaMKII expressed in the heart, allowing it to modulate many other Ca^{2+}-handling proteins including PLB, RyR, and L-type Ca channels (58). CaMKIIδ plays a key role in several types of heart disease including IR, and CaMKII inhibition is protective against IR-induced cell death and contractile dysfunction (35, 59). In miR-214 KO mice, elevated CaMKIIδ levels could therefore contribute to additional cardiomyocyte loss.

Ca^{2+} overload activates both apoptotic and necrotic pathways of cell death. Ischemic injury in the heart is accompanied by decreased expression of Bcl-2 and increased expression of proapoptotic Bcl-2 family members that modulate mitochondria-dependent apoptosis (26, 60). For example, mice lacking BNIP3, a proapoptotic family member, show decreased apoptosis and left ventricular remodeling following IR injury (61). Our data suggest that another proapoptotic Bcl-2 family member, BIM, is elevated in the miR-214 KO heart and may be a target of miR-214. While the role of BIM has not been extensively studied in the heart, data suggest it is regulated during ischemic injury and that its decreased expression hallmarks the rescue of cardiomyocyte apoptosis following IR (62, 63).

Ca^{2+} overload also stimulates necrotic cell death through opening of the MPT pore, which has recently been shown to play a major role in heart failure (39, 40). CypD (the *Ppif* gene product), a prolyl isomerase, is a key regulatory component of the MPT pore. *Ppif* KO mice are protected from Ca^{2+} overload and oxidative induced cell death and therefore are resistant to IR-induced cardiac injury (39). In contrast, mice that overexpress CypD show spontaneous cell death. We show increased CypD expression in miR-214 KO hearts at baseline and in cardiomyocytes with depleted miR-214, suggesting together with our luciferase data that *Ppif* is a direct miR-214 target and may sensitize KO cardiomyocytes to Ca^{2+} overload–mediated cell death. We did not observe elevated protein levels of CypD in miR-214 KO hearts at 7 days after IR. We speculate that a miR-214–independent mechanism allows for repression of CypD following IR to protect the heart from further cell death and loss of contractility.

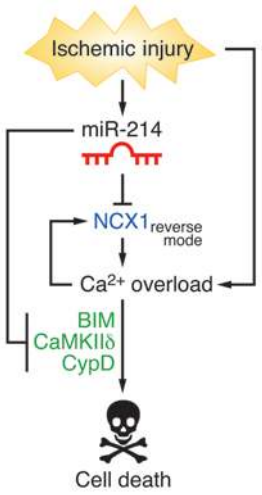

Figure 8
Model demonstrating miR-214 cardioprotection against Ca^{2+} overload injury and cell death. Ischemic injury leads to Ca^{2+} overload, causing a switch to reverse mode NCX1 activity in cardiomyocytes that enhances Ca^{2+} overload and leads to cell death via downstream effectors of Ca^{2+} signaling. miR-214, also induced by ischemic injury, protects the myocyte from damage by attenuating NCX1 levels to prevent excessive Ca^{2+} influx into the cytoplasm. Additional protection by miR-214 occurs through suppression of the Ca^{2+} effector kinase CaMKII and the cell death mediators CypD and BIM. In the absence of miR-214 expression in the heart, higher levels of reverse mode NCX1 and Ca^{2+} effectors further perpetuate Ca^{2+} overload and cell death during IR, resulting in greater impairment of cardiac function.

Significance of miRNAs in cardiac IR. Several miRNAs are regulated in response to IR injury (reviewed in ref. 23) and are reported to modulate cardiomyocyte cell death and contractility (20). However, the studies reported here are the first to our knowledge to address miRNA regulation of IR using both in vitro models and genetic deletion in mice. miR-21 has also been postulated to play a protective role in the heart during IR or hypoxic injury, based on studies performed with cardiomyocytes in vitro or using antagomiR against miR-21 (17, 64). In contrast, genetic deletion of miR-21 or knockdown with LNA-antimiRs has no affect on ischemic injury (65), highlighting the need to investigate the biology of miRNAs using genetic models.

In conclusion, the results of this study suggest that miR-214 protects the heart against IR injury by blunting Ca^{2+} overload and cell death in response to injury through its repression of NCX1, CaMKIIδ, CypD, and BIM. To our knowledge, these findings provide the first evidence for an important role of a miRNA in direct modulation of cardiac Ca^{2+} handling. Given that overexpression of NCX1 and intracellular Ca^{2+} overload also underlie cardiac hypertrophy and other forms of heart disease (66, 67), it is likely that miR-214 plays a cardioprotective role in a variety of stress settings. Thus, boosting miR-214 levels to attenuate Ca^{2+} overload and cardiac cell death may provide therapeutic benefit.

Methods

Northern blot analysis. Total RNA was isolated from mouse tissues, and miRNAs were detected as previously described (5). ^{32}P-labeled StarFire oligonucleotide probes (IDT) against mature miR-214 and miR-199a were used in the hybridization. U6 was used as a loading control.

Western blot analysis. Western blotting was performed according to standard protocols. See Supplemental Methods for details.

RT-PCR and qPCR analysis. qPCR for miR-214 and miR-199a was performed according to the manufacturer's protocol using the TaqMan miRNA assay kits (ABI). The relative quantities of miRNAs were normalized to RNU6B.

RT-PCR was performed using random hexamer primers with the Superscript III kit (Invitrogen). qPCR was performed using TaqMan probes (ABI).

Qualitative RT-PCR to assess Dnm3os splicing. RNA isolated from miR-214 KO hearts and WT littermates was subjected to RT-PCR, and then cDNA was amplified by PCR with 5 different primer sets spanning the *Dnm3os* transcript. Amplified products from WT and KO hearts were separated by gel electrophoresis side-by-side to visualize differences in size. See Supplemental Methods for primer sets used.

Generation of miR-214 KO mice. The targeting vector for generating a conditional allele of miR-214 mutation was constructed using the pGKneo-F2L2dta vector. The miR-214 targeting strategy was designed to replace the pre-miR-214 sequence with the neomycin resistance cassette flanked by loxP sites. See Supplemental Methods for details.

Histology and immunohistochemistry. H&E and Masson's trichrome stainings were performed using standard procedures. Wheat germ agglutinin staining was done on heart sections to assess cardiomyocyte size, and TUNEL staining was performed using the In Situ Cell Death Detection kit (Roche) according to the manufacturer's instructions. See Supplemental Methods for details.

Transthoracic echocardiography. Cardiac function and heart dimensions were evaluated by two-dimensional echocardiography using a Visual Sonics Vevo 2100 Ultrasound on conscious mice. See Supplemental Methods for details.

Electron microscopy. Samples were processed by the University of Texas Southwestern Medical Center Electron Microscopy Core facility. See Supplemental Methods for details.

Microarray analysis. For the microarray, P14 or adult heart RNA was pooled from 3 wild-type and 3 miR-214 KO animals. Microarray analysis was performed by the University of Texas Southwestern Microarray Core Facility using the Mouse Genome Illumina Mouse-6 V2 BeadChip. Data were deposited in NCBI's Gene Expression Omnibus (accession #GSE35421). See Supplemental Methods for details.

Cell culture, transfection, and luciferase assays. Cell culture, transfection, and luciferase studies were performed as previously described (7). See Supplemental Methods for details.

Neonatal rat cardiomyocyte culture and in vitro IR assays. See Supplemental Methods for cardiomyocyte isolation. To simulate IR in vitro, cardiomyocytes plated on coverslips were transfected with LNA-modified antimiRs, washed, and placed in DMEM containing no serum or supplements. Cells were placed in the hypoxia chamber for either 2 hours of ischemia (5% CO_2, 1% O_2) followed by 24 hours of reperfusion (mild IR) or 1 hour of anoxia (5% CO_2, 0% O_2) followed by 4 hours of reperfusion (severe IR). Coverslips were processed for TUNEL staining as described above and counterstained with Hoechst to visualize nuclei. Samples were run in triplicate, and 5–6 10× fields were imaged per coverslip.

Mouse model of MI and IR. Eight- to 12-week-old miR-214 KO male mice or WT controls were subjected to permanent (MI) or transient (IR) ligation of the LAD. See Supplemental Methods for details.

Adult mouse cardiomyocyte isolation and intracellular calcium ($[Ca2+]_i$) measurements. Cardiomyocytes from 8- to 10-week-old male mice were isolated by using enzymatic digestion and mechanical dispersion methods as described in detail in Supplemental Methods.

Mitochondrial respiratory activity and superoxide production. Mitochondrial electron transport activity and superoxide production were assessed as described in detail in Supplemental Methods.

Statistics. Results are expressed as the mean ± SEM. We used a 2-tailed, unpaired Student's *t* test for all pairwise comparisons (GraphPad Prism version 5). *P* values less than 0.05 were considered significant.

Study approval. All animal procedures were approved by the Institutional Animal Care and Use Committee of University of Texas Southwestern Medical Center.

Acknowledgments

We are grateful to Christopher Gilpin and the University of Texas Southwestern Medical Center (UTSW) Electron Microscopy Core for the EM images. We thank the UTSW Microarray Core Facility for Illumina microarray data and analysis. We thank Gaile Vitug and John Shelton for technical assistance and Jose Cabrera for graphics. Work in the laboratory of E.N. Olson was supported by grants from the NIH, the Donald W. Reynolds Center for Clinical Cardiovascular Research, the Robert A. Welch Foundation (grant I-0025), the Foundation Leducq's Transatlantic Network of Excellence in Cardiovascular Research Program, the American Heart Association–Jon Holden DeHaan Foundation, and the Cancer Prevention & Research Institute of Texas (CPRIT). A.B. Aurora was supported by an American Cancer Society Fellowship (grant PF-06-256-01-CSM).

Received for publication June 2, 2011, and accepted in revised form February 1, 2012.

Address correspondence to: Eric N. Olson, Department of Molecular Biology, 5323 Harry Hines Blvd, Dallas, Texas 75390-9148, USA. Phone: 214.648.1187; Fax: 214.648.1196; E-mail: eric.olson@utsouthwestern.edu.

1. Roger VL, et al. Heart disease and stroke statistics — 2011 update: a report from the American Heart Association. *Circulation*. 2011;123(4):e18–e209.
2. Small EM, Olson EN. Pervasive roles of microRNAs in cardiovascular biology. *Nature*. 2011; 469(7330):336–342.
3. Ikeda S, et al. MicroRNA-1 negatively regulates expression of the hypertrophy-associated calmodulin and Mef2a genes. *Mol Cell Biol*. 2009;29(8):2193–2204.
4. Zhao Y, et al. Dysregulation of cardiogenesis, cardiac conduction, and cell cycle in mice lacking miRNA-1-2. *Cell*. 2007;129(2):303–317.
5. van Rooij E, et al. A signature pattern of stress-responsive microRNAs that can evoke cardiac hypertrophy and heart failure. *Proc Natl Acad Sci U S A*. 2006;103(48):18255–18260.
6. Lin Z, Murtaza I, Wang K, Jiao J, Gao J, Li PF. miR-23a functions downstream of NFATc3 to regulate cardiac hypertrophy. *Proc Natl Acad Sci U S A*. 2009;106(29):12103–12108.
7. van Rooij E, Sutherland LB, Qi X, Richardson JA, Hill J, Olson EN. Control of stress-dependent cardiac growth and gene expression by a microRNA. *Science*. 2007;316(5824):575–579.
8. Callis TE, et al. MicroRNA-208a is a regulator of cardiac hypertrophy and conduction in mice. *J Clin Invest*. 2009;119(9):2772–2786.
9. da Costa Martins PA, et al. MicroRNA-199b targets the nuclear kinase Dyrk1a in an auto-amplification loop promoting calcineurin/NFAT signalling. *Nature Cell Biol*. 2010;12(12):1220–1227.
10. Thum T, et al. MicroRNA-21 contributes to myocardial disease by stimulating MAP kinase signalling in fibroblasts. *Nature*. 2008;456(7224):980–984.
11. Roy S, et al. MicroRNA expression in response to murine myocardial infarction: miR-21 regulates fibroblast metalloprotease-2 via phosphatase and tensin homologue. *Cardiovasc Res*. 2009;82(1):21–29.
12. van Rooij E, et al. Dysregulation of microRNAs after myocardial infarction reveals a role of miR-29 in cardiac fibrosis. *Proc Natl Acad Sci U S A*. 2008; 105(35):13027–13032.
13. Matkovich SJ, et al. MicroRNA-133a protects against myocardial fibrosis and modulates electrical repolarization without affecting hypertrophy in pressure-overloaded adult hearts. *Circulation Res*. 2010;106(1):166–175.
14. Fish JE, et al. miR-126 regulates angiogenic signaling and vascular integrity. *Dev Cell*. 2008;15(2):272–284.
15. Wang S, et al. The endothelial-specific microRNA miR-126 governs vascular integrity and angiogenesis. *Dev Cell*. 2008;15(2):261–271.
16. Bonauer A, et al. MicroRNA-92a controls angiogenesis and functional recovery of ischemic tissues in mice. *Science*. 2009;324(5935):1710–1713.
17. Sayed D, et al. MicroRNA-21 is a downstream effector of AKT that mediates its antiapoptotic effects via suppression of Fas ligand. *J Biol Chem*. 2010; 285(26):20281–20290.
18. Ye Y, Hu Z, Lin Y, Zhang C, Perez-Polo JR. Downregulation of microRNA-29 by antisense inhibitors and a PPAR-gamma agonist protects against myocardial ischaemia-reperfusion injury. *Cardiovasc Res*. 2010;87(3):535–544.
19. Wang JX, et al. miR-499 regulates mitochondrial dynamics by targeting calcineurin and dynamin-related protein-1. *Nat Med*. 2011;17(1):71–78.
20. Ren XP, et al. MicroRNA-320 is involved in the regulation of cardiac ischemia/reperfusion injury by targeting heat-shock protein 20. *Circulation*. 2009;119(17):2357–2366.
21. Wang X, et al. MicroRNA-494 targeting both proapoptotic and antiapoptotic proteins protects against ischemia/reperfusion-induced cardiac injury. *Circulation*. 2010;122(13):1308–1318.
22. Yellon DM, Hausenloy DJ. Myocardial reperfusion injury. *N Engl J Med*. 2007;357(11):1121–1135.
23. Ye Y, Perez-Polo JR, Qian J, Birnbaum Y. The role of microRNA in modulating myocardial ischemia-reperfusion injury. *Physiol Genomics*. 2011; 43(10):534–542.
24. Terentyev D, et al. miR-1 overexpression enhances Ca(2+) release and promotes cardiac arrhythmogenesis by targeting PP2A regulatory subunit B56alpha and causing CaMKII-dependent hyperphosphorylation of RyR2. *Circ Res*. 2009;104(4):514–521.
25. Rane S, et al. Downregulation of miR-199a derepresses hypoxia-inducible factor-1alpha and Sirtuin 1 and recapitulates hypoxia preconditioning in cardiac myocytes. *Circ Res*. 2009;104(7):879–886.
26. Dorn GW 2nd. Apoptotic and non-apoptotic programmed cardiomyocyte death in ventricular remodelling. *Cardiovasc Res*. 2009;81(3):465–473.
27. Murphy E, Steenbergen C. Mechanisms underlying acute protection from cardiac ischemia-reperfusion injury. *Physiol Rev*. 2008;88(2):581–609.
28. Ghali JK, et al. A phase 1-2 dose-escalating study evaluating the safety and tolerability of istaroxime and specific effects on electrocardiographic and hemodynamic parameters in patients with chronic heart failure with reduced systolic function. *Am J Cardiol*. 2007;99(2A):47A–56A.
29. Micheletti R, et al. Istaroxime, a stimulator of sarcoplasmic reticulum calcium adenosine triphosphatase isoform 2a activity, as a novel therapeutic approach to heart failure. *Am J Cardiol*. 2007;99(2A):24A–32A.
30. Mentzer RM Jr, et al. Sodium-hydrogen exchange inhibition by cariporide to reduce the risk of ischemic cardiac events in patients undergoing coronary artery bypass grafting: results of the EXPEDITION study. *Ann Thorac Surg*. 2008;85(4):1261–1270.
31. Talukder MA, Zweier JL, Periasamy M. Targeting calcium transport in ischaemic heart disease. *Cardiovasc Res*. 2009;84(3):345–352.
32. Frey N, McKinsey TA, Olson EN. Decoding calcium signals involved in cardiac growth and function. *Nat Med*. 2000;6(11):1221–1227.
33. Piper HM, Meuter K, Schafer C. Cellular mechanisms of ischemia-reperfusion injury. *Ann Thorac Surg*. 2003;75(2):S644–S648.
34. Backs J, Song K, Bezprozvannaya S, Chang S, Olson EN. CaM kinase II selectively signals to histone deacetylase 4 during cardiomyocyte hypertrophy. *J Clin Invest*. 2006;116(7):1853–1864.
35. Vila-Petroff M, et al. CaMKII inhibition protects against necrosis and apoptosis in irreversible ischemia-reperfusion injury. *Cardiovasc Res*. 2007; 73(4):689–698.
36. Currie S, Smith GL. Calcium/calmodulin-dependent protein kinase II activity is increased in sarcoplasmic reticulum from coronary artery ligated rabbit hearts. *FEBS Lett*. 1999;459(2):244–248.
37. Zamzami N, Kroemer G. The mitochondrion in apoptosis: how Pandora's box opens. *Nat Rev Mol Cell Biol*. 2001;2(1):67–71.
38. Halestrap AP. Calcium, mitochondria and reperfusion injury: a pore way to die. *Biochem Soc Trans*. 2006; 34(pt 2):232–237.
39. Baines CP, et al. Loss of cyclophilin D reveals a critical role for mitochondrial permeability transition in cell death. *Nature*. 2005;434(7033):658–662.
40. Nakayama H, et al. Ca2+- and mitochondrial-dependent cardiomyocyte necrosis as a primary mediator of heart failure. *J Clin Invest*. 2007;117(9):2431–2444.
41. Park CY, Choi YS, McManus MT. Analysis of microRNA knockouts in mice. *Hum Mol Genet*. 2010; 19(R2):R169–R175.
42. Juan AH, Kumar RM, Marx JG, Young RA, Sartorelli V. Mir-214-dependent regulation of the polycomb protein Ezh2 in skeletal muscle and embryonic stem cells. *Mol Cell*. 2009;36(1):61–74.
43. Flynt AS, Li N, Thatcher EJ, Solnica-Krezel L, Patton JG. Zebrafish miR-214 modulates Hedgehog signaling to specify muscle cell fate. *Nat Genet*. 2007;39(2):259–263.
44. Watanabe T, et al. Dnm3os, a non-coding RNA, is required for normal growth and skeletal development in mice. *Dev Dyn*. 2008;237(12):3738–3748.
45. Sipido KR, Maes M, Van de Werf F. Low efficiency of Ca2+ entry through the Na(+)-Ca2+ exchanger as trigger for Ca2+ release from the sarcoplasmic reticulum. A comparison between L-type Ca2+ current and reverse-mode Na(+)-Ca2+ exchange. *Circ Res*. 1997;81(6):1034–1044.
46. Flesch M, et al. Evidence for functional relevance of an enhanced expression of the Na(+)-Ca2+ exchanger in failing human myocardium. *Circulation*. 1996;94(5):992–1002.
47. Cross HR, Lu L, Steenbergen C, Philipson KD, Murphy E. Overexpression of the cardiac Na+/Ca2+ exchanger increases susceptibility to ischemia/reperfusion injury in male, but not female, transgenic mice. *Circ Res*. 1998;83(12):1215–1223.
48. Roos KP, et al. Hypertrophy and heart failure in

mice overexpressing the cardiac sodium-calcium exchanger. *J Card Fail*. 2007;13(4):318–329.
49. Reuter H, Han T, Motter C, Philipson KD, Goldhaber JI. Mice overexpressing the cardiac sodium-calcium exchanger: defects in excitation-contraction coupling. *J Physiol*. 2004;554(pt 3):779–789.
50. Kent RL, et al. Rapid expression of the Na(+)-Ca2+ exchanger in response to cardiac pressure overload. *Am J Physiol*. 1993;265(3 pt 2):H1024–H1029.
51. Menick DR, et al. The exchanger and cardiac hypertrophy. *Ann N Y Acad Sci*. 1996;779:489–501.
52. Sipido KR, Volders PG, Vos MA, Verdonck F. Altered Na/Ca exchange activity in cardiac hypertrophy and heart failure: a new target for therapy? *Cardiovasc Res*. 2002;53(4):782–805.
53. Wang J, et al. Induced overexpression of Na+/Ca2+ exchanger transgene: altered myocyte contractility, [Ca2+]i transients, SR Ca2+ contents, and action potential duration. *Am J Physiol Heart Circ Physiol*. 2009;297(2):H590–H601.
54. Yao A, Matsui H, Spitzer KW, Bridge JH, Barry WH. Sarcoplasmic reticulum and Na+/Ca2+ exchanger function during early and late relaxation in ventricular myocytes. *Am J Physiol*. 1997; 273(6 pt 2):H2765–H2773.
55. Reuter H, Han T, Motter C, Philipson KD, Gldhaber JI. Mice overexpressing the cardiac sodium-calcium exchanger: defects in excitation-contraction coupling. *J Physiol*. 2004;554(pt 3):779–789.
56. Kent RL, et al. Rapid expression of the Na(+)-Ca2+ exchanger in response to cardiac pressure overload. *Am J Physiol*. 1993;265(3 pt 2):H1024–H1029.
57. Menick DR, et al. The exchanger and cardiac hypertrophy. *Ann N Y Acad Sci*. 1996;779:489–501.
58. Anderson ME. Calmodulin kinase signaling in heart: an intriguing candidate target for therapy of myocardial dysfunction and arrhythmias. *Pharmacol Ther*. 2005;106(1):39–55.
59. Yang Y, et al. Calmodulin kinase II inhibition protects against myocardial cell apoptosis in vivo. *Am J Physiol Heart Circ Physiol*. 2006;291(6):H3065–H3075.
60. Chen Y, Lewis W, Diwan A, Cheng EH, Matkovich SJ, Dorn GW 2nd. Dual autonomous mitochondrial cell death pathways are activated by Nix/BNip3L and induce cardiomyopathy. *Proc Natl Acad Sci U S A*. 2010;107(20):9035–9042.
61. Diwan A, Wansapura J, Syed FM, Matkovich SJ, Lorenz JN, Dorn GW 2nd. Nix-mediated apoptosis links myocardial fibrosis, cardiac remodeling, and hypertrophy decompensation. *Circulation*. 2008; 117(3):396–404.
62. Bhuiyan MS, Takada Y, Shioda N, Moriguchi S, Kasahara J, Fukunaga K. Cardioprotective effect of vanadyl sulfate on ischemia/reperfusion-induced injury in rat heart in vivo is mediated by activation of protein kinase B and induction of FLICE-inhibitory protein. *Cardiovasc Ther*. 2008;26(1):10–23.
63. Bhuiyan MS, et al. Cytoprotective effect of bis(1-oxy-2-pyridinethiolato)oxovanadiun(IV) on myocardial ischemia/reperfusion injury elicits inhibition of Fas ligand and Bim expression and elevation of FLIP expression. *Eur J Pharmacol*. 2007;571(2–3):180–188.
64. Cheng Y, et al. Ischaemic preconditioning-regulated miR-21 protects heart against ischaemia/reperfusion injury via anti-apoptosis through its target PDCD4. *Cardiovasc Res*. 2010;87(3):431–439.
65. Patrick DM, et al. Stress-dependent cardiac remodeling occurs in the absence of microRNA-21 in mice. *J Clin Invest*. 2010;120(11):3912–3916.
66. Menick DR, et al. Regulation of Ncx1 gene expression in the normal and hypertrophic heart. *Ann N Y Acad Sci*. 2007;1099:195–203.
67. Xu L, et al. Chronic administration of KB-R7943 induces up-regulation of cardiac NCX1. *J Biol Chem*. 2009;284(40):27265–27272.